nature materials

LETTERS

PUBLISHED ONLINE: 6 FEBRUARY 2011 | DOI: 10.1038/NMAT2958

Orbital reflectometry of oxide heterostructures

Eva Benckiser[1], Maurits W. Haverkort[1], Sebastian Brück[2,3], Eberhard Goering[2], Sebastian Macke[2], Alex Frañó[1], Xiaoping Yang[1,4], Ole K. Andersen[1], Georg Cristiani[1], Hanns-Ulrich Habermeier[1], Alexander V. Boris[1], Ioannis Zegkinoglou[1], Peter Wochner[2], Heon-Jung Kim[1,5], Vladimir Hinkov[1]* and Bernhard Keimer[1]*

The occupation of *d* orbitals controls the magnitude and anisotropy of the inter-atomic electron transfer in transition-metal oxides and hence exerts a key influence on their chemical bonding and physical properties[1]. Atomic-scale modulations of the orbital occupation at surfaces and interfaces are believed to be responsible for massive variations of the magnetic and transport properties[2–8], but could not thus far be probed in a quantitative manner[9–11]. Here we show that it is possible to derive quantitative, spatially resolved orbital polarization profiles from soft-X-ray reflectivity data, without resorting to model calculations. We demonstrate that the method is sensitive enough to resolve differences of ∼3% in the occupation of Ni e_g orbitals in adjacent atomic layers of a $LaNiO_3$–$LaAlO_3$ superlattice, in good agreement with *ab initio* electronic-structure calculations. The possibility to quantitatively correlate theory and experiment on the atomic scale opens up many new perspectives for orbital physics in transition-metal oxides.

The electronic properties of transition-metal oxides (TMOs) are determined by the interplay of the spin, charge and orbital degrees of freedom of the valence electrons. Progress in understanding and predicting these properties relies on quantitative experimental information about the spatial variation of all three observables on the atomic scale. Powerful probes of the spin and charge densities are already available. For instance, neutron diffractometry and reflectometry are routinely used to determine the magnetization profiles in the bulk and near surfaces and interfaces, respectively. The valence-electron charge density is more difficult to investigate, because most scattering probes couple to the total charge that is dominated by the core electrons. Recently, however, spectroscopic methods such as electron energy-loss spectroscopy[12] and soft-X-ray reflectometry[13] have yielded atomically resolved profiles of the valence-electron charge.

The *d*-orbital degree of freedom is the distinguishing characteristic of TMOs compared with materials with valence electrons in the *s*- and *p*-electron shells. In bulk TMOs, spatial variations of the *d*-orbital occupation are known to generate a multitude of electronic phases with radically different macroscopic properties[1], and the influence of 'orbital reconstructions' on the physical properties of surfaces and interfaces is currently a subject of intense investigation[2–8]. At present, however, only the spatial average of the orbital occupation can be determined in a facile and quantitative manner, by means of X-ray linear dichroism (XLD), a method that relies on the excitation of core electrons into the valence *d* orbitals by linearly polarized photons[14]. Despite its obvious scientific interest, quantitative experimental information about spatial variations of the *d*-orbital polarization is very limited. Methods used to determine site-specific variations of the orbital occupation in the bulk are mostly qualitative and/or require extensive model calculations that add substantial uncertainties[9–11]. Even less information is available on orbital polarization profiles near surfaces and interfaces. Some evidence of orbital reconstructions near single TMO interfaces has been derived from comparison of XLD measurements in different detection modes[2] and from comparison with corresponding bulk data[5–7], but these methods do not provide depth resolution.

Here we focus on TMO interfaces, which are currently at the centre of a large-scale research effort driven by prospects to control and ultimately design their electronic properties[15]. As the orbital occupation determines the electronic bandwidth and the magnetic exchange interactions at and near the interfaces, detailed experimental information on the orbital polarization is essential for the design of suitable heterostructures. We show that quantitative, depth-resolved profiles of the orbital occupation in TMO heterostructures and superlattices can be derived from linearly polarized X-ray reflectometry with photon energies near transition-metal *L*-absorption edges. The orbital occupation is extracted by the application of sum rules, analogous to XLD, so model calculations are not required. The method is broadly applicable to TMO surfaces and interfaces and can be readily generalized to bulk diffractometry.

We demonstrate the new method by an investigation of a superlattice composed of the paramagnetic metal $LaNiO_3$ (LNO) and the band insulator $LaAlO_3$ (LAO). The Ni^{3+} ion in LNO has a $3d^7$ electron configuration, and the nearly cubic crystal field of the perovskite structure splits the atomic $3d$ orbital manifold into a lower-lying triply degenerate t_{2g} level occupied by six electrons and a higher-lying doubly degenerate e_g level with a single electron. Whereas in bulk LNO the two Ni e_g orbitals (with x^2-y^2 and $3z^2-r^2$ symmetry) are equally occupied, model calculations have suggested that the x^2-y^2 (in-plane) orbital can be stabilized by epitaxial strain and confinement in a superlattice geometry (Fig. 1), and that the electronic structure of superlattices with fully polarized in-plane orbitals matches that of the copper oxide high-temperature superconductors[16–18]. This system is thus a prime candidate for 'orbitally engineered' superconductivity.

We have used pulsed laser deposition to grow a (4 u.c.//4 u.c.) ×8 LNO–LAO superlattice on a $SrTiO_3$ (STO) substrate (u.c., pseudo-cubic unit cell; see Fig. 1). As the lattice constant of

[1]Max Planck Institute for Solid State Research, Heisenbergstraße 1, 70569 Stuttgart, Germany, [2]Max Planck Institute for Metals Research, Heisenbergstraße 3, 70569 Stuttgart, Germany, [3]Experimentelle Physik 4, Physikalisches Institut, Am Hubland, 97074, Würzburg, Germany, [4]Division of Materials Science, Nanyang Technological University, 50 Nanyang Avenue, 639798, Singapore, [5]Department of Physics, Daegu University, Jillyang, Gyeongsan 712-714, South Korea. *e-mail: v.hinkov@fkf.mpg.de; b.keimer@fkf.mpg.de.

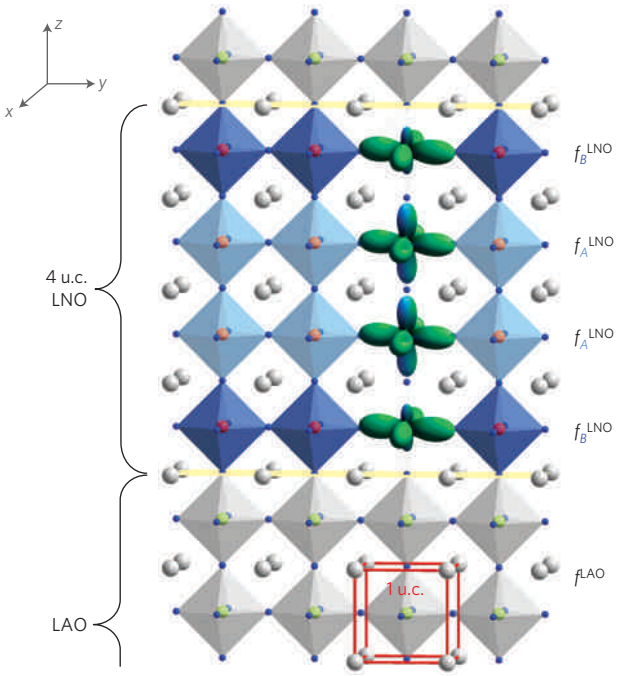

Figure 1 | Sketch of the LNO–LAO superlattice with layer stacks of four pseudo-cubic unit cells (u.c., see the red box) investigated in this work. The modulation of the Ni 3*d* e_g orbital occupation along the superlattice normal *z* is depicted by a different mixture of x^2–y^2 and $3z^2$–r^2 orbitals and modelled with different scattering tensors $f_{A/B}^{LNO}$ (see the text). The orbital occupation imbalance has been overstated for clarity.

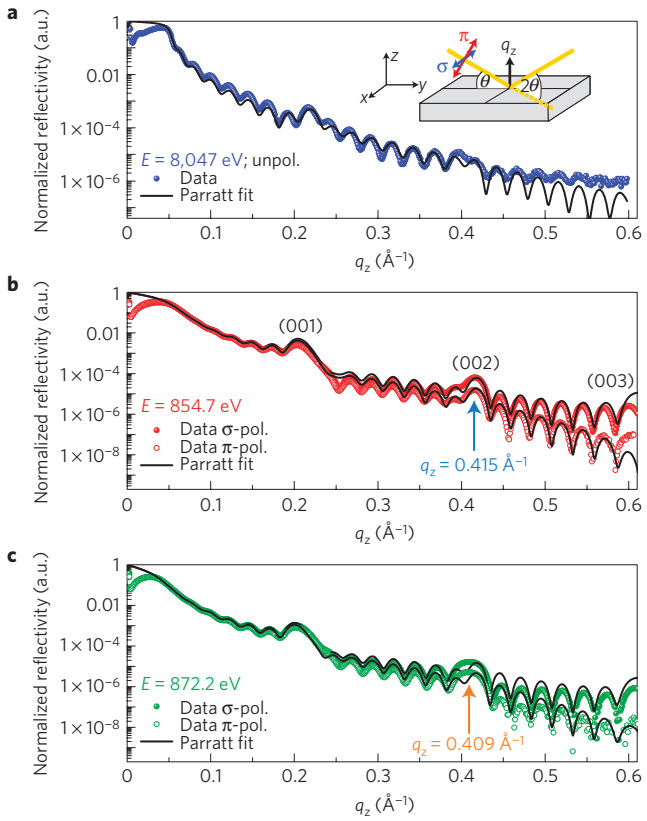

Fit parameters	Thickness (Å)	Roughness (Å)
7 bilayer LAO/LNO (coupled)	15.2/15.4	3.5/2.0
STO substrate	∞	1.7
LNO buffer layer	18.5	3.3
LAO cap layer	18.3	3.0

Figure 2 | Momentum-dependent X-ray reflectivity of the (4 u.c.//4 u.c.) × 8 LNO–LAO superlattice. a–c, Reflectivity for $E = 8,047$ eV (Cu Kα; hard X-rays) (**a**), $E = 854.7$ eV (Ni L_3) (**b**) and $E = 872.2$ eV (Ni L_2) (**c**). All data have been normalized to unity at $q_z = 0$. The measurements in the soft-X-ray range have been made with σ- and π-polarization of the incident X-rays (see the sketch in **a**). The solid black line is the best fit to the data when using the Parratt algorithm. The fitted parameters, roughness and thickness, are summarized in the table below. The estimated error bars of the individual thicknesses and roughnesses are approximately ±0.5 Å.

cubic STO is somewhat larger than the pseudo-cubic lattice constants of LNO and LAO (mismatch ∼2%), the superlattice is expected to be under tensile strain. The high crystalline quality and strain state of the sample were verified by X-ray diffraction and reciprocal-space mapping (see Supplementary Information). Transport[19] and optical ellipsometry measurements in combination with low-energy muon spin rotation (Boris, A. V. *et al.* unpublished) show that 4-u.c.-thick LNO layer stacks in TMO superlattices are metallic and paramagnetic. The total thickness of 247 ± 8 Å of the superlattice was chosen to ensure that the sample is thin enough to clearly resolve total-thickness fringes, but thick enough to minimize contributions of Ni^{2+} that might occur in the vicinity of the polar layer–substrate interface[20].

The reflectivity measurements were made at room temperature in specular geometry, that is, the momentum transfer q was parallel to the surface normal z (see the Methods section). The resulting data for photon energy 8,047 eV, far from resonance in the hard-X-ray range (Fig. 2a), reflect the high quality of the investigated superstructure. At energies corresponding to the Ni $L_{2,3}$ resonances at 854.7 eV and 872.2 eV, we observe superlattice peaks up to the third order, denoted by SL (00l), $l = 1, 2, 3$ in Fig. 2. To obtain the layer thickness and interface roughness of our superlattice, we fitted the q-dependent data using our newly developed reflectivity analysis program ReMagX (ref. 21) in a mode based on the Parratt formalism[22] (for details see Supplementary Information). The resulting profiles are shown in Fig. 2, and the structural parameters are given in the table below. The best fit is obtained when allowing the first LNO layer stack (buffer layer) grown on STO and the last LAO layer stack (cap layer) to be slightly thicker and different in roughness. We stress that our structural model is simple and gives an excellent description for the full set of data, measured for different energies and polarization geometries.

The X-ray absorption spectra (XAS) measured in total-electron yield (TEY) and fluorescence-yield (FY) modes are shown in Fig. 3a. Owing to the vicinity of the strong La M_4 white lines, the Ni L_3 line is only seen as a shoulder around 855 eV (see the inset), but the Ni L_2 white line is clearly observed at 872 eV. The FY data show a smaller intensity at the La white lines and an enhanced contribution at the Ni lines compared with the TEY. This is explained by self-absorption effects, limited energy resolution, different probing depths of the two methods and the fact that the topmost layer of the superlattice is an LAO layer. However, the dichroic difference spectrum clearly shows dips at the Ni L_3 and L_2 white-line energies, which we attribute to natural linear dichroism (Fig. 3c). We obtained nearly identical results from FY and TEY data (not shown for clarity).

In general, natural linear dichroism reflects an anisotropy of the charge distribution around a particular ion[14]. To obtain a quantitative estimate of the imbalance in e_g band occupation in our

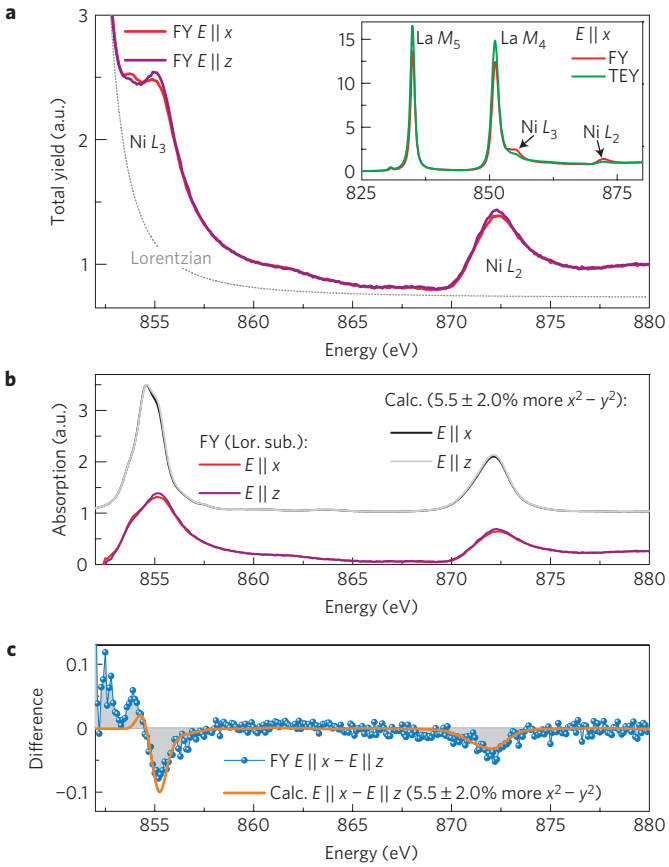

Figure 3 | Polarization-dependent XAS spectrum (FY) across the Ni $L_{2,3}$ edges. a, XAS spectra for $E \parallel x$ (in-plane) and $E \parallel z$ (out-of-plane) polarization. In the inset we compare TEY and FY spectra for $E \parallel x$ in the full energy range including the La $M_{4,5}$ white lines. **b**, Polarized FY spectra after subtraction of a Lorentzian profile fitted to the La M_4 line shown together with results for Ni^{3+} XAS spectra with 5.5% higher x^2–y^2 occupation, obtained from the cluster calculation. **c**, Difference spectra ($E \parallel x$–$E \parallel z$) calculated from the measured (blue points) and calculated (orange line) data shown in the middle panel.

superlattice, we applied the sum rule for linear dichroism[23,24], which relates the total integrated intensity of the polarized spectra ($I_{E\parallel x,z}$) to the hole occupation $\underline{n}_{3z^2-r^2}$ and $\underline{n}_{x^2-y^2}$ in the e_g orbitals:

$$\frac{\underline{n}_{3z^2-r^2}}{\underline{n}_{x^2-y^2}} = \frac{3I_{E\parallel z}}{4I_{E\parallel x} - I_{E\parallel z}}$$

By integrating the spectra in the range 853–877 eV, after subtracting the La M_4 contribution estimated by a Lorentzian profile (Fig. 3b), we obtain $\underline{n}_{3z^2-r^2}/\underline{n}_{x^2-y^2} = 1.030(5)$. We define the orbital polarization

$$P = \frac{(n_{x^2-y^2} - n_{3z^2-r^2})}{(n_{x^2-y^2} + n_{3z^2-r^2})} \qquad (1)$$

with $n_{x^2-y^2}$ and $n_{3z^2-r^2}$ being the numbers of electrons, and finally obtain $P = 5 \pm 2\%$. The effect of covalency would slightly reduce this number, but this effect is within the quoted error bar and is hence ignored. To confirm these results and obtain a description of the lineshape of the polarized XAS spectra, we carried out a cluster calculation for a Ni^{3+} ion in an almost-cubic crystal field of six oxygen ions ($\Delta e_g = 10$ meV; see Fig. 3b; ref. 25). Although the cluster calculation is expected to give good results for localized electrons in insulators, we expect some deviations in the calculated lineshape of the XAS spectra in the case of our metallic nickelate layers. Indeed, although we included reasonable line broadening (due to the finite temperature and experimental resolution), the measured lineshape is not fully reproduced, and we show the best result scaled to the experimental data in such a way that the integrated spectral weight is conserved. However, as pointed out above, the polarization dependence of the spectra is independent of details in lineshape. To reproduce the measured dichroic difference, $P = 5.5 \pm 2\%$ higher x^2–y^2 band occupation is needed, in good agreement with the result obtained from the sum rule. In particular, we stress that a higher occupation of the $3z^2$–r^2 band would result in a sign change of the XLD signal and can be excluded.

Although in XAS the averaged absorption of the LNO layers is measured, that is, XAS $\propto 1/\omega \mathrm{Im}(f_A^{LNO} + f_B^{LNO})$, where ω denotes the photon frequency, for LNO layer stacks composed of two inner layers with scattering factor f_A^{LNO} and two interface layers with f_B^{LNO} (see Fig. 1), the intensity of the (002) superlattice reflection of a symmetric superlattice is mainly determined by the difference $F^{(002)} \propto (1-i)(f_B^{LNO} - f_A^{LNO})$. Taking advantage of this relation, we studied the polarization dependence of the reflected intensity across the Ni L edge for momentum transfers q_z in the vicinity of the (002) superlattice peak (Fig. 4). First, we notice that the lineshape of the scattering profiles is rather different compared with the XAS profiles and strongly depends on q_z. Second, there is a pronounced polarization dependence, which only occurs at the Ni (L_3 and L_2) edge energies. In particular, the single-peak profile observed for σ polarization is split into a double-peak profile for π-polarized photons. Although the relative intensities change somewhat with q_z, nearly identical difference spectra are observed for both q_z values. A qualitative comparison with the dichroic signal observed in the absorption spectra already shows a clear enhancement, which indicates a modulation of orbital occupancy within the LNO layer stack.

To confirm this conclusion and extract quantitative information about the orbital occupation, we used the newly developed analysis tool[21] to simulate the constant-q_z scans (right-hand panels of Fig. 4), on the basis of the structural parameters derived from q_z-dependent reflectometry and the optical constants obtained from FY-XAS (see Supplementary Information for details). To model the observed polarization dependence, a dielectric tensor of at least tetragonal symmetry has to be taken into account, which calls for an analysis beyond the conventional Parratt formalism. Within the framework of the optical approach for multilayers, we implemented formulae from the magneto-optical formalism derived in ref. 26. We modelled our data with LNO layer stacks split into four unit-cell-thick layers, labelled A and B in the following (Fig. 1). For each layer A and B we assumed a dielectric tensor with tetragonal symmetry of the form

$$\hat{\varepsilon}_{\mathrm{tetra\ A(B)}}{}^{\mathrm{LNO}} = \begin{pmatrix} \varepsilon_{\mathrm{A(B)}}{}^{xx} & 0 & 0 \\ 0 & \varepsilon_{\mathrm{A(B)}}{}^{xx} & 0 \\ 0 & 0 & \varepsilon_{\mathrm{A(B)}}{}^{zz} \end{pmatrix} \qquad (2)$$

with complex entries $\varepsilon^{jj} = \varepsilon_1{}^{jj} + i\varepsilon_2{}^{jj}$ ($j = x, z$) related to the scattering factors f_A^{LNO} and f_B^{LNO} (see Supplementary Information for details). In the case of a homogeneous LNO stack with B and A layer with the same dichroism, the measured averaged dichroism was taken as input, that is, ε^{xx} and ε^{zz} obtained from the XAS for $E \parallel x$ and $E \parallel z$, respectively. The simulated constant-q_z scans for the homogeneous LNO stack cannot reproduce the large anisotropy observed in the experiment (see light-blue/orange lines in the right-hand panels of Fig. 4). We therefore considered the case of a modulated LNO stack with different x^2–y^2 band occupations in layers A and B, keeping the averaged dichroism of $5.5 \pm 2\%$ obtained from XLD fixed. To model the optical constants, we

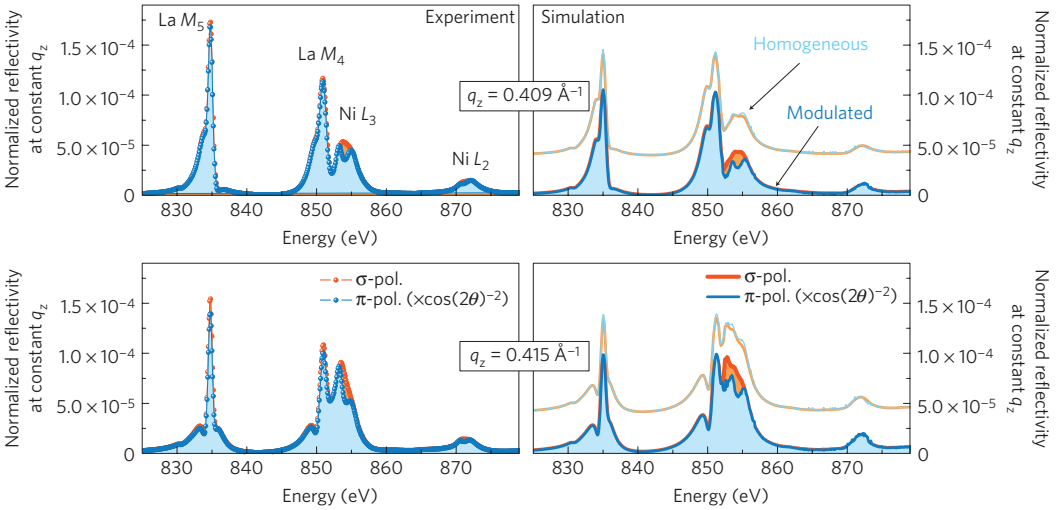

Figure 4 | Energy scans of the reflectivity data with constant momentum transfer q_z. Two q_z values close to the (002) superlattice peak have been chosen from the q-dependent profiles (Fig. 2): $q_z = 0.409$ Å^{-1} (top panels) and $q_z = 0.415$ Å^{-1} (bottom panels). The left-hand panels show the polarization-dependent experimental data. The right-hand panels show the corresponding simulated curves for LNO layers with (1) homogeneous orbital occupation within the LNO layer stack (shifted by 4×10^{-5} for clarity) and (2) modulated orbital occupation of $P_B = 7 \pm 3\%$ higher x^2–y^2 band occupation in the interface layers and $P_A = 4 \pm 1\%$ higher x^2–y^2 band occupation in the inner layers. Experimental data and simulations are shown for σ- and π-polarization of the incoming photons. To correct for the difference in absolute reflected intensity for σ- and π-polarization due to the vicinity of the Brewster angle, we multiplied the data for π-polarization by the factor $\cos(2\theta)^{-2}$ obtained by approximation from the Fresnel formulae.

parameterized them in the following way: for the cubic case the tensor has diagonal entries $\varepsilon_{\mathrm{cubic}} = 1/3(2\varepsilon^{xx} + \varepsilon^{zz})$. Using this and the parameter $\alpha \in [0, 1]$ we can write the tensor elements:

$$(\varepsilon_{\mathrm{tetra\ A(B)}}{}^{\mathrm{LNO}})_{jj} = (1 \mp \alpha)\varepsilon^{jj} \pm \alpha\varepsilon_{\mathrm{cubic}}$$

with upper signs for layer A and lower ones for layer B, and ε^{jj} as defined in equation (2). The parameter α measures the degree of orbital polarization of layers A and B with the constraint that the total orbital polarization obtained from XAS is fixed. For $\alpha = 0$ layer B is equivalent to layer A, both with 5.5% higher x^2–y^2 occupancy (homogeneous case), whereas for $\alpha = 1$ layer B has 11% higher x^2–y^2 occupancy and layer A is cubic (maximally modulated case). By varying the parameter α we obtained different optical input data, which we used to calculate the constant-q_z profiles around (002) (see Supplementary Information). When comparing the normalized difference spectra of the constant-q_z scans, we found the best agreement of simulations and experiment for $\alpha = 0.3 \pm 0.05$ and a stacking sequence BAAB. This corresponds to a $P_B = 7 \pm 3\%$ higher x^2–y^2 population in the interface layers B and a $P_A = 4 \pm 1\%$ higher x^2–y^2 population in the inner layers A. There is a clear difference to the solution with stacking ABBA (see Supplementary Information).

To compare our results with the predictions of *ab initio* electronic-structure calculations[16–18], we have carried out LDA + U calculations for the particular superlattice geometry studied in this work with 4 u.c. LNO (for details see Supplementary Information). Using equation (1), we obtain an orbital polarization of 6% (3%) for the outer (inner) NiO_2 layers B (A), in excellent agreement with the experimental result. On the basis of these LDA + U studies we can attribute the layer-dependent modulation of the orbital occupancy to a difference in the bonding patterns of Ni ions in inner and outer layers. As the bonding pattern is bulk-like in the inner layers, the relatively small orbital polarization is mostly due to strain. For Ni ions in the outer layers, on the other hand, the kinetic-energy gain by out-of-plane hopping across the interface is suppressed owing to the closed-shell configuration of the neighbouring Al^{3+} ion and its reduced hybridization with oxygen. This explains the preferential occupation of the in-plane orbital in Ni ions adjacent to the LAO layer.

We conclude that polarized resonant X-ray reflectometry in combination with the analysis method we have presented here is a powerful tool to accurately map out the orbital-occupation profile in TMO multilayers. The quantitative correspondence between theoretical predictions and experimental measurements that we have demonstrated opens up new perspectives for the synthesis of TMO interfaces and superlattices with designed electronic properties, including but not limited to the nickelate system we have investigated here. Potential tuning parameters for a systematic design effort include epitaxial strain from the substrate and the constituents of the superlattice, the thicknesses of the individual layers and the covalency of the chemical bonds across the interface. Finally, we note that the methodology introduced here can be readily generalized to other systems with non-uniform orbital occupation, such as surfaces and bulk systems with staggered orbital order, and thus has the potential to bring orbital physics in TMOs to a new level of quantitative accuracy.

Methods

High-quality superlattices with atomic-scale precision have been grown by pulsed-laser deposition from LNO and LAO stoichiometric targets using a KrF excimer laser with 2 Hz pulse rate and 1.6 J cm^{-2} energy density. Both compounds were deposited in 0.5 mbar oxygen atmosphere at 730 °C and subsequently annealed in 1 bar oxygen atmosphere at 690 °C for 30 min. Here we investigated a (4 u.c.//4 u.c.) × 8 LNO–LAO superlattice grown on an atomically flat [001]-oriented single-crystalline STO substrate. The crystallinity, superlattice structure and sharpness of the interfaces (roughness ≤1 u.c.) were verified by high-resolution hard-X-ray diffraction along the specular rod. Reciprocal-space mapping around the (103) STO peak shows that the strain induced by the substrate is partially relaxed within a total thickness of 247 Å (see Supplementary Information for details).

The resonant X-ray reflectivity and XAS measurements were carried out at UE56/2-PGM1 soft-X-ray beam line at BESSY II in Berlin, Germany, using the advanced three-axis ultrahigh-vacuum reflectometer described in ref. 27. The undulator beamline supplies 90% linearly σ- and π-polarized light (for the notation see the sketch in Fig. 2a). Beamline settings have been chosen to result in a bandwidth of 0.57 eV at 840 eV (optimized intensity). The X-ray absorption profiles were measured with σ- and π-polarization of the incident light at an angle of incidence of $\theta = 30°$. Although for σ-polarization the measured intensity corresponds directly to $E \parallel x$, the intensity for $E \parallel z$ is

deduced from $I_z = 4/3I_\pi - 1/3I_x$, with I_π being the measured intensity with π-polarization[28]. Reflected intensities have been measured with a diode and were corrected by the fluorescence background, measured independently with a second diode. All intensities have been normalized by the incoming intensity measured with a gold mesh.

Density functional calculations were carried out using the Vienna *Ab Initio* Simulation Package code. The projector augmented plane-wave[29,30] method was used in the framework of the generalized gradient approximation[31–34]. The orbital occupation numbers were obtained by integrating the projected density of states within a fixed sphere on Ni x^2-y^2 or $3z^2-r^2$ orbitals (see Supplementary Information for details).

Received 25 August 2010; accepted 7 January 2011; published online 6 February 2011

References

1. Tokura, Y. & Nagaosa, N. Orbital physics in transition-metal oxides. *Science* **288,** 462–468 (2000).
2. Chakhalian, J. *et al.* Orbital reconstruction and covalent bonding at an oxide interface. *Science* **318,** 1114–1117 (2007).
3. Rata, A. D. *et al.* Strain-induced insulator state and giant gauge factor of $La_{0.7}Sr_{0.3}CoO_3$ films. *Phys. Rev. Lett.* **100,** 076401 (2008).
4. Jackeli, G. & Khaliullin, G. Spin, charge, and orbital order at the interface between correlated oxides. *Phys. Rev. Lett.* **101,** 216804 (2008).
5. Tebano, A. *et al.* Evidence of orbital reconstruction at interfaces in ultrathin $La_{0.67}Sr_{0.33}MnO_3$ films. *Phys. Rev. Lett.* **100,** 137401 (2008).
6. Aruta, C. *et al.* Orbital occupation, atomic moments, and magnetic ordering at interfaces of manganite thin films. *Phys. Rev. B* **80,** 014431 (2009).
7. Salluzzo, M. *et al.* Orbital reconstruction and the two-dimensional electron gas at the $LaAlO_3/SrTiO_3$ interface. *Phys. Rev. Lett.* **102,** 166804 (2009).
8. Yu, P. *et al.* Interface ferromagnetism and orbital reconstruction in $BiFeO_3$–$La_{0.67}Sr_{0.33}MnO_3$ heterostructures. *Phys. Rev. Lett.* **105,** 027201 (2010).
9. Schlappa, J. *et al.* Direct observation of t_{2g} orbital ordering in magnetite. *Phys. Rev. Lett.* **100,** 026406 (2008).
10. Thomas, K. J. *et al.* Soft X-ray resonant diffraction study of magnetic and orbital correlations in a manganite near half doping. *Phys. Rev. Lett.* **92,** 237204 (2004).
11. Wilkins, S. B. *et al.* Direct observation of orbital ordering in $La_{0.5}Sr_{1.5}MnO_4$ using soft X-ray diffraction. *Phys. Rev. Lett.* **91,** 167205 (2003).
12. Muller, D. A. Structure and bonding at the atomic scale by scanning transmission electron microscopy. *Nature Mater.* **8,** 263–270 (2009).
13. Smadici, S. *et al.* Superconducting transition at 38 K in insulating-overdoped La_2CuO_4–$La_{1.64}Sr_{0.36}CuO_4$ superlattices: Evidence for interface electronic redistribution from resonant soft X-ray scattering. *Phys. Rev. Lett.* **102,** 107004 (2009).
14. Stöhr, J. & Siegmann, H. C. *Magnetism. From Fundamentals to Nanoscale Dynamics* (Springer, 2007).
15. Mannhart, J. & Schlom, D. G. Oxide interfaces—an opportunity for electronics. *Science* **327,** 1607–1611 (2010).
16. Chaloupka, J. & Khaliullin, G. Orbital order and possible superconductivity in $LaNiO_3/LaMO_3$ superlattices. *Phys. Rev. Lett.* **100,** 016404 (2008).
17. Hansmann, P. *et al.* Turning a nickelate Fermi surface into a cupratelike one through heterostructuring. *Phys. Rev. Lett.* **103,** 016401 (2009).
18. Han, M. J., Marianetti, C. A. & Millis, A. J. Chemical control of orbital polarization in artificially structured transition-metal oxides: La_2NiXO_6 (X = B, Al, Ga, In) from first principles. *Phys. Rev. B* **82,** 134408 (2010).
19. May, S. J., Santos, T. S. & Bhattacharya, A. Onset of metallic behaviour in strained $(LaNiO_3)_n/(SrMnO_3)_2$ superlattices. *Phys. Rev. B* **79,** 115127 (2009).
20. Liu, J. *et al.* Effect of polar discontinuity on the growth of $LaNiO_3/LaAlO_3$ superlattices. *Appl. Phys. Lett.* **96,** 133111 (2010).
21. Macke, S., Brück, S. & Goering, E. ReMagX X-ray magnetic reflectivity tool, www.mf.mpg.de/remagx.html.
22. Parratt, L. G. Surface studies of solids by total reflection of X-rays. *Phys. Rev.* **95,** 359–369 (1954).
23. Thole, B. T. & van der Laan, G. Sum rules for magnetic dichroism in rare earth 4*f* photoemission. *Phys. Rev. Lett.* **70,** 2499–2502 (1993).
24. van der Laan, G. Sum rules and fundamental spectra of magnetic X-ray dichroism in crystal field symmetry. *J. Phys. Soc. Jpn.* **63,** 2393–2400 (1994).
25. Schüßler-Langeheine, C. *et al.* Spectroscopy of stripe order in $La_{1.8}Sr_{0.2}NiO_4$ using resonant soft X-ray diffraction. *Phys. Rev. Lett.* **95,** 156402 (2005).
26. Višňovský, Š. Magneto-optical polar Kerr effect and birefringence in magnetic crystals of orthorhombic symmetry. *Czech. J. Phys. B* **34,** 155–162 (1984).
27. Brück, S., Bauknecht, S., Ludescher, B., Goering, E. & Schütz, G. An advanced magnetic reflectometer. *Rev. Sci. Instrum.* **79,** 083109 (2008).
28. Wu, W. B. *et al.* Orbital polarization of $LaSrMnO_4$ studied by soft X-ray linear dichroism. *J. Electron Spectroscopy* **137–140,** 641–645 (2004).
29. Blöchl, P. E. Projector augmented-wave method. *Phys. Rev. B* **50,** 17953–17979 (1994).
30. Kresse, G. & Joubert, D. From ultrasoft pseudopotentials to the projector augmented-wave method. *Phys. Rev. B* **59,** 1758–1775 (1999).
31. Perdew, J. P., Burke, K. & Ernzerhof, M. Generalized gradient approximation made simple. *Phys. Rev. Lett.* **77,** 3865–3868 (1996).
32. Perdew, J. P., Burke, K. & Ernzerhof, M. Erratum: Generalized gradient approximation made simple. *Phys. Rev. Lett.* **77,** 3865 (1996); *Phys. Rev. Lett.* **78,** 1396 (1997).
33. Kresse, G. & Hafner, J. *Ab initio* molecular-dynamics simulation of the liquid-metal–amorphous-semiconductor transition in germanium. *Phys. Rev. B* **49,** 14251–14269 (1994).
34. Kresse, G. & Furthmüller, J. Efficient iterative schemes for *ab initio* total-energy calculations using a plane-wave basis set. *Phys. Rev. B* **54,** 11169–11186 (1996).

Acknowledgements

We acknowledge financial support from the Deutsche Forschungsgemeinschaft within the framework of the TRR80, project C1. The authors thank G. Khaliullin, V. Kiryukhin, and G. A. Sawatzky for discussions. We acknowledge the provision of synchrotron radiation and the assistance from W. Mahler and B. Zada at the UE562-PGM1 beamline at Helmholtz-Zentrum Berlin—BESSY II. We thank M. Dudek for making the hard-X-ray reflectivity measurements, and S. Heinze for taking the atomic force microscopy image.

Author contributions

E.B. carried out the experiments and analysed the data. M.W.H. made substantial contributions to the data analysis and carried out the cluster calculations. S.B. and E.G. designed and set the experiment up. S.B., E.G. and S.M. developed the analysis tool ReMagX. G.C. and H-U.H. grew the superlattices by pulsed laser deposition. A.F., E.B., A.V.B. and P.W. characterized the samples by high-resolution X-ray diffraction. X.Y. and O.K.A. carried out the LDA + *U* calculations. I.Z. and H.J.K. assisted in the experiments. V.H. worked on the data collection and analysis. E.B., M.W.H., V.H. and B.K. wrote the paper. V.H. and B.K. coordinated the project.

Additional information

The authors declare no competing financial interests. Supplementary information accompanies this paper on www.nature.com/naturematerials. Reprints and permissions information is available online at http://npg.nature.com/reprintsandpermissions. Correspondence and requests for materials should be addressed to V.H. or B.K.